Copper Binding Affinity of S100A13, a Key Component of the FGF-1 Nonclassical Copper-Dependent Release Complex

Vaithiyalingam Sivaraja,* Thallapuranam Krishnaswamy Suresh Kumar,* Dakshinamurthy Rajalingam,* Irene Graziani,† Igor Prudovsky,† and Chin Yu*‡

*Department of Chemistry and Biochemistry, University of Arkansas, Fayetteville, Arkansas; †Center for Molecular Medicine, Maine Medical Center Research Institute, Scarborough, Maine; and ‡Department of Chemistry, National Tsing Hua University, Hsinchu, Taiwan

ABSTRACT S100A13 is a member of the S100 protein family that is involved in the copper-dependent nonclassical secretion of signal peptideless proteins fibroblast growth factor 1 and interleukin 1α. In this study, we investigate the effects of interplay of Cu^{2+} and Ca^{2+} on the structure of S100A13 using a variety of biophysical techniques, including multi-dimensional NMR spectroscopy. Results of the isothermal titration calorimetry experiments show that S100A13 can bind independently to both Ca^{2+} and Cu^{2+} with almost equal affinity (K_d in the micromolar range). Terbium binding and isothermal titration calorimetry data reveal that two atoms of Cu^{2+}/Ca^{2+} bind per subunit of S100A13. Results of the thermal denaturation experiments monitored by far-ultraviolet circular dichroism, limited trypsin digestion, and hydrogen-deuterium exchange (using ^{1}H-^{15}N heteronuclear single quantum coherence spectra) reveal that Ca^{2+} and Cu^{2+} have opposite effects on the stability of S100A13. Binding of Ca^{2+} stabilizes the protein, but the stability of the protein is observed to decrease upon binding to Cu^{2+}. ^{1}H-^{15}N chemical shift perturbation experiments indicate that S100A13 can bind simultaneously to both Ca^{2+} and Cu^{2+} and the binding of the metal ions is not mutually exclusive. The results of this study suggest that the Cu^{2+}-binding affinity of S100A13 is important for the formation of the FGF-1 homodimer and the subsequent secretion of the signal peptideless growth factor through the nonclassical release pathway.

INTRODUCTION

S100 proteins are the largest family within the EF-hand protein super-family (1,2). S100 proteins are acidic proteins of small molecular mass (~10–12 kDa), devoid of disulfide bonds. They contain two EF-hands, an S100-specific EF-hand located at the N-terminal end followed by a classical Ca^{2+}-binding EF-hand (3–6). S100 proteins have been implicated in Ca^{2+} homeostasis and a wide array of Ca^{2+}-dependent signaling pathways that regulate important cellular processes such as differentiation, development, and tumor growth (7–9). S100 proteins exhibit distinct cell- and tissue-specific expression and are believed to be involved in a multitude of human diseases such as cystic fibrosis, cardiomyopathy, rheumatoid arthritis, and several types of cancer (10–14).

To date, S100A13 is the only member of the S100 family that is known to exhibit ubiquitous expression in a broad range of tissues (10,14). Unlike other S100 proteins, which exhibit positive cooperativity for the four calcium binding sites in their dimeric structure, S100A13 contains two Ca^{2+} binding sites with distinctly different affinities (14,15). In addition, in typical S100 proteins, the binding of Ca^{2+} leads to opening of EF-hand domains, which in turn renders large hydrophobic surface(s) accessible to the solvent (5,16). The solvent-exposed hydrophobic domain(s) provides a binding surface for the protein-protein interaction (2,7,16). In marked contrast, the Ca^{2+}-free apo-form of S100A13 shows solvent-exposed hydrophobic pockets (14,15). Conversely, in the presence of calcium, a drastic decrease in the solvent-accessible nonpolar surface(s) is observed (14,15,17). Therefore, it is believed that the molecular mechanism of activation of S100A13 is distinctly different from that of other S100 proteins. S100A13 is known to be involved in the nonclassical export of signal peptideless proteins such as fibroblast growth factor (FGF-1) and interleukin 1α (15,18,19). Formation of the multi-protein release complex, consisting of FGF-1, S100A13, and the p40 form of synaptotagmin 1 (p40 Syt1) is crucial for the nonclassical secretion of FGF-1 (18).

Several studies have demonstrated that copper ions (Cu^{2+}) play a vital role in the organization of the FGF-1 multi-protein release complex (18,20,21). Depletion of Cu^{2+} using a specific chelator, tetrathiomolybdate, is shown to inhibit the stress-induced release of FGF-1 (20,21). Cu^{2+} is believed to be crucial for the formation of the covalent FGF-1 homodimer that is present in the multi-protein complex (18). It has been demonstrated that the homodimerization of FGF-1 mediated by cysteine 30 is critical for FGF-1 release (20,21). Additionally, Cu^{2+} ions induce noncovalent binding between FGF-1, S100A13, and p40 Syt1 (20). However, the primary source of Cu^{2+} ions required for the formation of the FGF-1 homodimer is still not clear. Interestingly, in addition to Ca^{2+}, many members of the S100 protein family bind to other metals, such as zinc and copper (22). These

Submitted December 22, 2005, and accepted for publication May 22, 2006.

Address reprint requests to T. K. S. Kumar, Dept. of Chemistry and Biochemistry, University of Arkansas, Fayetteville, AR 72701. Tel.: 479-5755646; Fax: 479-5754049; E-mail: sthalla@uark.edu; or to Chin Yu, Dept. of Chemistry, National Tsing Hua University, Hsinchu, Taiwan 300. Tel.: 886-35-721524; Fax: 886-35-711082; E-mail: cyu@mx.nthu.edu.tw.

0006-3495/06/09/1832/12 $2.00

doi: 10.1529/biophysj.105.079988

transition metal ions are believed to play a regulatory role by modulating the affinity of various S100 proteins for Ca^{2+} and/or protein targets (22). In this context, in the study described here, we investigate the affinity of S100A13 to Cu^{2+} ions and describe the structural interplay between Ca^{2+} and Cu^{2+} binding to the protein. The results obtained show that S100A13 binds to Cu^{2+} ions with high affinity. Cu^{2+} binds to dimeric S100A13 structures at a novel location connecting the N-terminus of one subunit with the hinge region of the other subunit. It appears that S100A13 can act as a source for Cu^{2+} ions required for the organization of the FGF-1 multiprotein release complex.

EXPERIMENTAL METHODS

Protein expression and purification

The amplified cDNA of S100A13 was inserted into a pGEX expression vector. The expression of S100A13 was carried out in *Escherichia coli*. ^{15}N-labeled protein was prepared by growing the cells in M9-minimal medium containing ^{15}N-labeled NH_4Cl as the sole source of nitrogen. The expressed glutathione S-transferase (GST)-fused S100A13 was purified on a GST column(s). Apo-S100A13 preparations were made by repeated dialysis of the protein against EDTA. The absence of the metal was verified by the isocompetition point mass. The GST tag was eliminated by thrombin (Sigma, St. Louis, MO) cleavage and the protein was repurified by affinity chromatography on GST-sepharose.

Isothermal titration calorimetry (ITC)

Metal binding to S100A13 was characterized by measuring the heat changes during the titration of the relevant metal chloride into the protein solution using Microcal VP titration calorimeter (Northampton, MA). S100A13 and metal chloride solutions were centrifuged and degassed under vacuum condition before titration. The sample cell contained 0.1 mM S100A13 dissolved in 25 mM Tris buffer (pH 7.2) containing 25 mM KCl. Solutions of 2 mM $CaCl_2$/$CuCl_2$ were prepared in the same buffer as used in the cell sample and the pH of the solutions was corrected to 7.2. Titrations were performed by injecting 5- to 10-μL aliquots of 2 mM ligand ($CaCl_2$/$CuCl_2$) into a 0.1-mM solution of S100A13. The titration of S100A13 with the C2A domain was performed at 25°C by dissolving both the proteins in 25 mM Tris buffer (pH 7.2) containing 25 mM KCl. Results of the titration curves were corrected using protein-free buffer control and analyzed using Origin software supplied by Microcal (Northampton, MA).

Fluorescence spectroscopy

Fluorescence experiments were carried out on a Hitachi F2500 spectrofluorimeter (Tokyo, Japan). The Tb^{3+} titration was carried out using a stock solution of 50 mM $TbCl_3$ containing 25 mM Tris (pH 7.2) and 25 mM KCl. All experiments were performed using a quartz cell with a light path of 10 mm and an excitation wavelength of 280 nm. Tb^{3+} emission spectra were acquired between 400 nm to 600 nm. The slit widths for emission and excitation were set at 2.5 nm and 10 nm, respectively. All experiments were carried out at a protein concentration of 50 μM.

8-anilino-1-naphthalenesulfonate binding experiments

The 8-anilino-1-naphthalenesulfonate (ANS) binding experiments were performed using a Hitachi F-2500 spectrofluorometer at 25°C. Fluorescence spectra were recorded using an excitation wavelength of 390 nm and an emission wavelength range of 400–600 nm. Ca^{2+} and Cu^{2+} were added from a 1-M stock solution of $CaCl_2$/$CuCl_2$ prepared in the storage buffer (pH 7.2) containing 25 mM KCl and 25 mM Tris (pH 7.2). Control experiments with ANS were carried out under the same buffer conditions, but in the absence of the protein. The final concentrations of the protein and ANS used were 50 μM and 250 μM, respectively.

Circular dichroism

The circular dichroism (CD) experiments were performed using a Jasco J-720 spectropolarimeter (Tokyo, Japan). All CD experiments were carried out at 100 μg/mL protein concentration. A 0.2-cm quartz cell was used for all the experiments and the signal was monitored in the wavelength range of 200–250 nm. Each spectrum represents an average of 10 scans.

Proteolytic digestion

Proteolytic digestion experiments were carried out at 25°C using trypsin (Sigma) as the proteolytic enzyme, in the absence or presence of the metal ions (at a metal ion(Cu^{2+}/Ca^{2+}) concentration of 2 mM). Proteolytic digestions were carried out at an enzyme/protein molar ratio of 1:10. The reaction was arrested at regular time intervals by the addition of the gel loading dye (Bio-Rad, Hercules, CA). The degree of proteolytic cleavage was estimated by densitometry of the intensity of the ~12-kDa band corresponding to the uncleaved S100A13. The intensity of the S100A13 band not subjected to the trypsin treatment was used as a control for 100% protection against trypsin cleavage.

NMR spectroscopy

NMR experiments were performed on a Bruker Avance DMX-700 MHz spectrometer (Billerica, MA) equipped with a 5-mm inverse cryoprobe. The protein samples were prepared in 25 mM d_6-Tris HCl containing 25 mM KCl, 2 mM $CaCl_2$/$CuCl_2$, and 0.03% NaN_3. The pH of all the samples was corrected to 7.2. All NMR data were acquired at 25°C and the data were analyzed using XWINNMR 3.5 software supplied by Bruker.

Hydrogen-deuterium exchange experiment

The protein samples (Ca^{2+}-bound or Cu^{2+}-bound S100A13 titrated with 2 mM $CaCl_2$) were lyophilized along with 25 mM Tris HCl and 25 mM KCl. The lyophilized powder was dissolved immediately in 0.55 mL of D_2O. The pH (7.2) was not corrected for deuterium effects. Data collection was initiated after 10 min of incubation of the protein in D_2O. The concentration of S100A13 used was 0.5 mM. The 600 ^1H-^{15}N heteronuclear single quantum coherence (HSQC) spectra were acquired continuously for a time period of 200 h. All data were analyzed using the Kaleidagraph software (Synergy Software, Philadelphia, PA).

RESULTS

Apo-state of S100A13 binds to both Ca^{2+} and Cu^{2+}

Isothermal titration calorimetry is an important tool for the direct measurement of thermodynamic parameters in various biological interactions (23). As ITC is dependent only on the exchange of heat during a reaction, it is an invaluable tool for monitoring a variety of reactions independent of spectroscopic changes. ITC has been successfully used not only to

quantitatively measure binding affinities between two interacting molecules but also to calculate various thermodynamic parameters, such as change in Gibbs free energy (ΔG), enthalpy change (ΔH), entropy change (ΔS), and specific heat capacity (ΔCp), that provide insights into the nature and magnitude of interactions that govern protein-protein or protein-metal interactions (24). It is in this context that we used ITC to characterize the binding affinity of S100A13 to metal ions such as Ca^{2+} and Cu^{2+}. The binding curve representing the interaction between apo-S100A13 and Ca^{2+} is almost hyperbolic (Fig. 1 *A*). The binding between apo-S100A13 and Ca^{2+} is exothermic and the reaction proceeds with a negative change in enthalpy. Best-fit of the binding isotherm yields apparent binding constant values of ~8 μM and ~66 μM (Table 1). The binding curve saturates at a Ca^{2+}/protein dimer ratio of 4:1. Recently, Arnesano et al., studying the affinity of human S100A13 to Cu^{2+}, reported that prior binding of Ca^{2+} is a prerequisite for the binding of Cu^{2+} to the protein (17). They suggested that binding of Ca^{2+} to S100A13 triggers a drastic conformational change creating a novel site for Cu^{2+}. The results of their study imply that Cu^{2+} cannot bind to apo-S100A13 independently of Ca^{2+}. To verify this observation, we investigated the binding affinity of apo-S100A13 to Cu^{2+}. Interestingly, the binding isotherm of apo-S100A13 with Cu^{2+} clearly shows that Cu^{2+} binds to apo-S100A13 (Fig. 1 *B*) and the binding constant values characterizing the apo-S100A13-Cu^{2+} interaction are ~12 μM and ~55 μM, respectively (Table 1). These results suggest that S100A13 binds to Ca^{2+} and Cu^{2+} with almost similar affinities. The binding curve saturates at Cu^{2+} to the S100A13 monomer ratio of 2:1, suggesting that four Cu^{2+} ions bind per molecule of the S100A13 dimer (Table 1). Thus, ITC data clearly show that apo-S100A13 binds to both Ca^{2+} and Cu^{2+}, and the binding of Cu^{2+} does not require the prior binding of Ca^{2+} to the protein.

Conformational changes monitored by ANS binding

The three-dimensional structures of S100 proteins are characterized by the presence of two EF-hands (2,3). Each EF-hand presents a helix-loop-helix structure (2). Ca^{2+} binding sites are located in the loop portions of the helix-loop-helix structures. Ca^{2+} binding decreases the flexibility of residues in the loop portion of the helix-loop-helix structure, and consequently a small β-sheet segment is induced in that region in most S100 proteins, including S100A13 (2,5; Sivaraja et al., unpublished results). In addition, binding of Ca^{2+} to S100 proteins is known to cause a significant change of the interhelical angle between helix-3 and helix-4 at the C-termini (5). These subtle secondary structural changes in S100A13 could not be clearly detected by conventional spectroscopic probes such as infrared spectroscopy and circular dichroism spectroscopy (15). Therefore, we used ANS binding experiments to monitor the conformational changes induced by metal ions (Ca^{2+}/Cu^{2+}) in S100A13.

ANS is a hydrophobic dye that has been successfully used to detect solvent-accessible hydrophobic surface(s) in proteins. Using ANS binding experiments we had previously shown that there are large areas of solvent-accessible nonpolar surfaces in apo-S100A13 (15). Presence of solvent-exposed nonpolar clefts in apo-S100A13 is manifested by an intense ANS emission signal that is blue-shifted by ~30 nm (from 520 nm in the absence of the protein to 490 nm in the

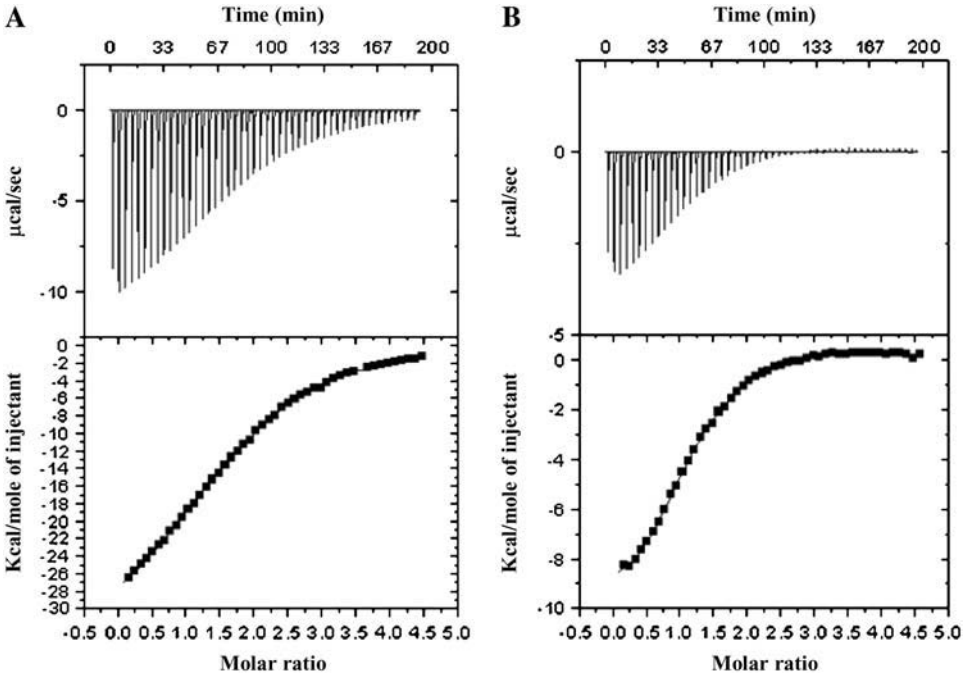

FIGURE 1 Isothermograms representing the binding of S100A13 to (*A*) Ca^{2+} and (*B*) Cu^{2+}. The upper panels represent the raw data and the bottom panels are the best fits of the raw data. The binding isotherms have been fit to the multiple binding sites model. The concentration of protein used was 100 μM in 25 mM Tris (pH 7.2) containing 25 mM KCl. Appropriate background corrections were made to account for the heats of dilution and ionization. All experiments were performed at 25°C.

TABLE 1 Binding parameters characterizing the S100A13-metal interation

Interaction type	Binding constant(μM)		ΔG_b(kcal mol^{-1})	N (number of binding sites per monomer)
	K_{d1}	K_{d2}		
apo-S100A13 + Ca^{2+}	8 ± 1	66 ± 1	−8.065 ± 0.5	2
apo-S100A13 + Cu^{2+}	12 ± 1	55 ± 1	−7.086 ± 0.5	2
Ca^{2+}-bound S100A13 + Cu^{2+}	62 ± 1	120 ± 1	−6.126 ± 0.5	2
Cu^{2+}-bound S100A13 + Ca^{2+}	7.6 ± 1	140 ± 1	−7.808 ± 0.5	2

presence of the protein). Addition of Ca^{2+} results in a progressive decrease in the emission intensity of the dye, suggesting a subtle conformational change resulting in the increase in the fraction of free ANS in the bulk polar solvent. (Fig. 2 *A*). This situation is in sharp contrast to that observed in other S100 proteins, wherein Ca^{2+} binding results in an increase in the solvent accessibility of nonpolar residues located in the cleft between helix-3 and helix-4 (comprising the C-terminal EF-hand (Ridinger et al. (14)). Typically, Ca^{2+}-bound states of S100 proteins recognize and bind to their target proteins through the solvent-exposed hydrophobic surfaces (3). The nonavailability of such solvent-accessible nonpolar surfaces in the Ca^{2+}-bound state of S100A13 suggests that its mechanism of activation and recognition of target protein partners is significantly different from other members of the S100 protein family.

It was interesting to examine whether Cu^{2+}, like Ca^{2+}, could also bring about subtle conformational changes that influence the solvent accessibility of hydrophobic residues in S100A13. Fig. 2 *B* shows that the emission intensity of ANS at 520 nm gradually decreases with an increase in the concentration of Cu^{2+}. The decrease in emission intensity is accompanied by a progressive red shift in the emission maxima of ANS from 490 nm to 508 nm, suggesting the burial of the nonpolar surface to the interior of the protein molecule. Increasing the Cu^{2+} concentration beyond 0.2 mM does not produce further appreciable decrease in the ANS emission intensity, indicating the saturation of the Cu^{2+}-mediated structural changes beyond this metal ion concentration (0.2 mM) (Fig. 2, *B* and *C*). Although both Ca^{2+} and Cu^{2+} promote the burial of the solvent-accessible nonpolar residues to the interior of the protein (S100A13), the degrees of exposure of the nonpolar residues to the solvent are possibly different in the Ca^{2+}- and Cu^{2+}-bound states of S100A13. The exposure of solvent-accessible nonpolar surface(s) is marginally higher in the Cu^{2+}-bound state than that observed in the Ca^{2+}-bound state of S100A13 (Fig. 2 *C*). Titration of the Cu^{2+}-bound S100A13 with increasing concentration of Ca^{2+} not only results in a gradual red shift in the emission maxima (from 480 nm to 500 nm) but also in a decrease in the emission intensity of the hydrophobic dye (at 520 nm, Fig. 2 *C*). Upon addition of 2 mM of Ca^{2+} to the Cu^{2+}-bound S100A13, the relative emission intensity of ANS (at 520 nm) matches quite well with that obtained upon binding to the protein in the presence of only Ca^{2+}. These results support our conclusion that the degree of solvent accessibility of the nonpolar surfaces in S100A13 is higher in the presence of Cu^{2+} than that observed in the presence of Ca^{2+}.

Detection of conformational changes using limited trypsin digestion

Limited protease digestion analysis is a valuable technique for probing conformational changes induced in a protein upon ligand binding (25). The factors that primarily influence protease-induced cleavage are solvent accessibility of the susceptible sites, their protrusion from the surface of the protein, hydrogen bonds between cleavage sites and the rest of the molecule, flexibility of the site, and its propensity to local unfolding/packing (26). In this background, we used limited trypsin-digestion analysis as a tool to probe the possible structural changes induced in S100A13 by metal ions (Ca^{2+} and Cu^{2+}). Trypsin generally cleaves proteins at the C-terminal ends of basic amino acids such as lysine and arginine. As S100A13 is rich in lysine and arginine residues, trypsin is an apt choice to monitor the conformational changes induced by the metal ions (Ca^{2+} and Cu^{2+}). The extent of proteolytic cleavage was monitored from the decrease in intensity of the 12-kDa Coomassie blue-stained band (on sodium dodecyl sulfate polyacrylamide gel electrophoresis (SDS-PAGE)) corresponding to uncleaved S100A13 (Fig. 3 *A*). Cleavage of apo-S100A13 occurs instantaneously upon addition of trypsin. More than 80% of the protein is cleaved within 70 min of initiation of the cleavage reaction (Fig. 3, *A* and *B*). In marked contrast, the Ca^{2+}-bound state of S100A13 is resistant to trypsin cleavage (Fig. 3, *A* and *B*). More than 90% of the S100A13 protein remains uncleaved after 70 min of initiation of the trypsin cleavage (Fig. 3). These results show that the protein assumes a more tightly packed conformation upon binding to Ca^{2+}. The degree of susceptibility of Cu^{2+}-bound S100A13 to trypsin cleavage is higher than observed in the Ca^{2+}-bound state of S100A13 (Fig. 3, *A* and *B*). In the presence of Cu^{2+}, >30% of the 12-kDa band (on SDS-PAGE) is cleaved after 90 min of the cleavage reaction (Fig. 3 *B*). The rate of trypsin-induced cleavage of Cu^{2+}-bound S100A13 is significantly higher than that observed in the Ca^{2+}-bound state of S100A13, but lower than in the apo-state of the protein (Fig. 3 *B*). Results of the trypsin digestion experiment clearly show that structures of the Ca^{2+} and Cu^{2+}-bound states of S100A13 are subtly different. The Ca^{2+}-bound state of S100A13 appears to be more tightly packed than the Cu^{2+}-bound form of the protein.

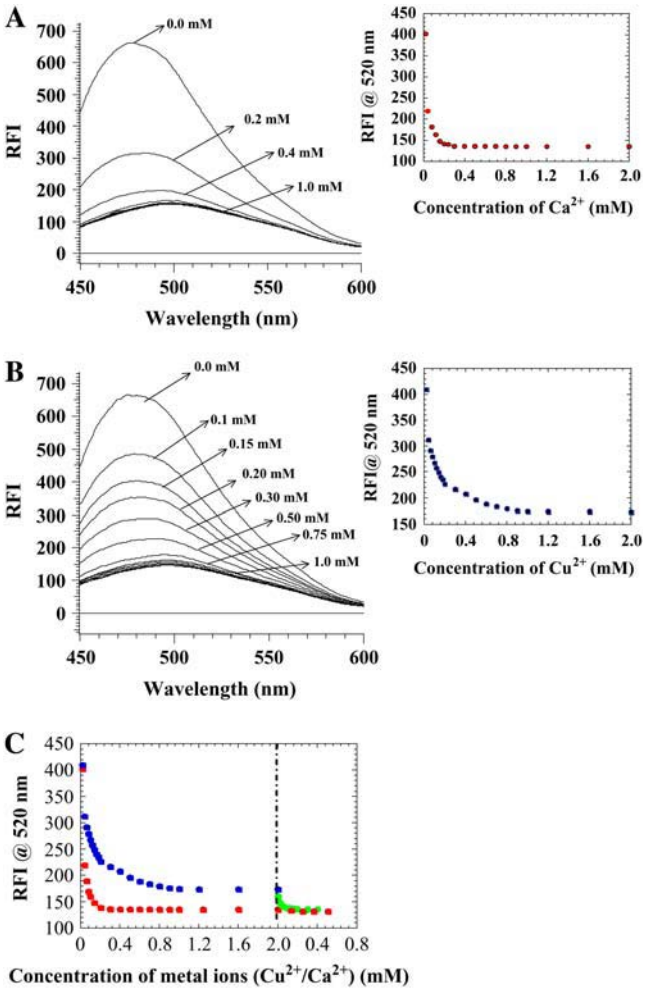

FIGURE 2 (*A*) Emission spectra of ANS in the presence of the S100A13 at various concentrations of Ca^{2+}. The inset figure shows the decrease in fluorescence intensity of ANS (at 520 nm) upon increasing the concentration of Ca^{2+}. (*B*) Emission spectra of ANS in the presence of S100A13 at various concentration of Cu^{2+}. The inset figure depicts the decrease in the ANS emission intensity (at 520 nm) as a function of the concentration of Cu^{2+}. (*C*) Changes in ANS emission intensity (at 520 nm) upon addition of Ca^{2+} alone (*red*) and Cu^{2+} alone (*blue*) to S100A13. The portion of the curve indicated in green shows the decrease in the ANS emission intensity when increasing amounts of Ca^{2+} (0–0.5 mM) are added to the Cu^{2+}-saturated (2 mM) S100A13. The concentrations of S100A13 and ANS used are 50 μM and 250 μM, respectively. Background corrections were made in all the spectra. The dashed line indicates the beginning of the titration of the Cu^{2+}-saturated (2 mM) S100A13 with increasing concentration of Ca^{2+}.

Conformational changes monitored by 2D NMR spectroscopy

^{1}H-^{15}N HSQC spectrum is a finger-print of the backbone conformation of a protein (27). Each ^{1}H-^{15}N crosspeak in the spectrum represents the microenvironment of an amino acid residue in a given conformation of the protein (27). Therefore, the conformational transitions induced by the metal ions (Ca^{2+}/Cu^{2+}) can be easily traced from the perturbation of the crosspeaks in the ^{1}H-^{15}N HSQC spectrum. The ^{1}H-^{15}N HSQC spectrum of apo-S100A13 is not well-dispersed and many crosspeaks in the spectrum are broadened (Fig. 4 *A*). We have been able to accomplish only partial assignment of the resonances in apo-S100A13. However, addition of Ca^{2+} drastically increases the dispersion of crosspeaks in the ^{1}H-^{15}N HSQC spectrum (Fig. 4 *B*). All the crosspeaks in the ^{1}H-^{15}N HSQC spectrum of the Ca^{2+}-bound state of S100A13 have been unambiguously assigned (28). The three-dimensional solution structure of the Ca^{2+}-bound S100A13 has been recently solved at high resolution (15). As mentioned earlier, β-sheet conformation is induced in the Ca^{2+}-binding site located in the loop portion of the helix-loop-helix structure (in the EF-hands). Residues involved in the calcium binding site in S100A13 include 24–29 and 34–37 in the N-terminal EF-hand, and 64–68 and 71–74 in the C-terminal EF-hand. Most of these residues constitute the new β-sheet segment induced upon Ca^{2+}-binding to S100A13. The crosspeaks of residues involved in the beta-sheet show good chemical shift dispersion in the ^{1}H-^{15}N HSQC spectrum. The transformation of the structureless loop to the β-sheet conformation is reflected in the emergence of new crosspeaks from the severely overlapped region(s) of the ^{1}H-^{15}N HSQC spectrum of S100A13 (Fig. 4 *B*). Increase in the interhelical angle between helices (H3 and H4 of the EF-hand) does not appear to cause significant chemical perturbation of crosspeaks in the ^{1}H-^{15}N HSQC spectrum. In summary, binding of Ca^{2+} to apo-S100A13 causes two major structural changes: 1), induction of β-sheet conformation in the loop region of the helix-loop-helix structure in both EF-hands; and 2), change in the interhelical angle between helices constituting the C-terminal EF-hand.

Copper (Cu^{2+}) is a paramagnetic and, therefore, if Cu^{2+} should bind to a protein, then the NMR signals at the metal (Cu^{2+}) binding site would be expected to broaden with the reciprocal of the sixth power of the metal-nucleus distance (29). There have been numerous studies wherein crosspeaks of residues (in the ^{1}H-^{15}N HSQC spectrum) that are within the vicinity of the Cu^{2+}-binding site(s) have been shown to decrease in intensity and subsequently disappear (30,31). Selected crosspeaks in the ^{1}H-^{15}N HSQC spectrum of apo-S100A13, acquired in the presence of 1 mM Cu^{2+}, show a progressive decrease in intensity upon addition of Cu^{2+}. Most of these crosspeaks are located in the crowded region(s) of the ^{1}H-^{15}N HSQC spectrum and hence could not be unambiguously assigned (Fig. 4 *C*). The dramatic increase in the chemical-shift dispersion of the crosspeaks in the ^{1}H-^{15}N HSQC spectrum observed when Ca^{2+} binds to the protein (S100A13) is not seen in the ^{1}H-^{15}N HSQC spectra of the Cu^{2+}-bound S100A13. The increased chemical-shift dispersion observed in the presence of Ca^{2+} is primarily attributed to the induction of β-sheet conformation at the Ca^{2+} binding site. Therefore, it appears that, unlike Ca^{2+}, the binding of Cu^{2+} to S100A13 does not induce new β-sheet conformation in the protein. Based on the analysis of ^{1}H-^{15}N chemical-shift perturbation, ITC, and ANS binding data, the following

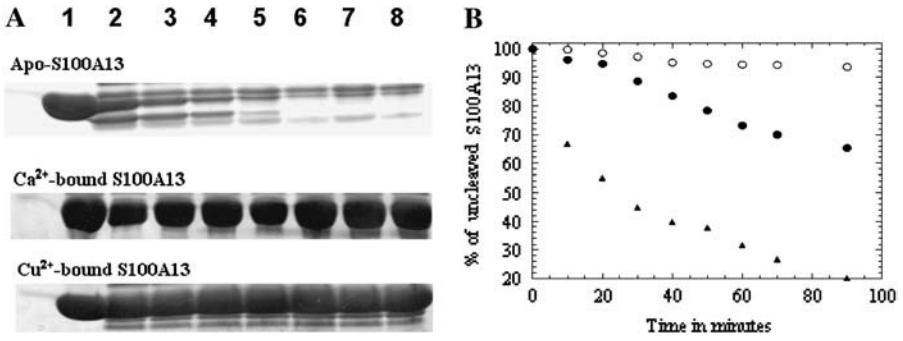

FIGURE 3 (*A*) SDS-PAGE analysis of the trypsin cleavage products of free S100A13 and S100A13 in the presence of metal ions (2 mM Ca^{2+}/Cu^{2+}). Lanes 1 to 8 indicate the progress of the trypsin-induced cleavage of S100A13 after 0 min, 10 min, 20 min, 30 min, 40 min, 50 min, 60minutes, and 70 min of incubation of the protein with the enzyme. (*B*) Percentage of uncleaved S100A13 in the absence of metal ions (*solid triangles*) in the presence of 2 mM Ca^{2+} (*open circles*) and in the presence of 2 mM Cu^{2+} (*solid circles*). The percentage of uncleaved S100A13 was estimated from the intensity of the 12.5-kDa Coomassie blue-stained band on polyacrylamide gel. The concentrations of S100A13 and trypsin used were 50 μM and 500 μM, respectively.

general conclusions could be drawn on the effects of binding of Cu^{2+} to apo-S100A13. 1), Two Cu^{2+} ions bind per subunit of apo-S100A13. However, it is not clear if the Cu^{2+} ions bind at the Ca^{2+}-binding sites or at sites remote from the Ca^{2+}-binding sites. 2), Unlike Ca^{2+}, binding of Cu^{2+} does not appear to lead to the induction of β-sheet conformation in the helix-loop-helix structure of the two EF-hands. 3), ANS binding data show that Cu^{2+} binding results in partial burial of the solvent-accessible nonpolar surfaces in the protein. However, the degree of accessibility of the nonpolar surface(s) in the Cu^{2+}-bound S100A13 structure is higher than that observed in the structure of the Ca^{2+}-bound S100A13.

Binding of Ca^{2+} and Cu^{2+} to S100A13 is not mutually exclusive

The results discussed thus far clearly show that S100A13 can bind to both Ca^{2+} and Cu^{2+}. In this context, it would be interesting to understand if these two metal ions compete for the same site(s) in the protein. ITC experiments, monitoring the titration of calcium-bound (2 mM Ca^{2+}) S100A13 with Cu^{2+} reveal that the binding of the two metal ions (Ca^{2+} and Cu^{2+}) is not mutually exclusive (Fig. 5 *A*). Although the apparent binding-constant values characterizing the binding of Cu^{2+} to the Ca^{2+}-bound S100A13 is marginally lower than that observed in the absence of Ca^{2+} (Table 1), the number of Cu^{2+} ions bound to the protein remains the same (two Cu^{2+} ions per monomer of the Ca^{2+}-bound S100A13). Similarly, the best-fit of the binding curve representing the titration of Cu^{2+}-bound S100A13 with Ca^{2+} shows that there are $\sim$2 Ca^{2+}-binding sites per subunit of the Cu^{2+}-bound S100A13 (Fig. 5 *B*). The binding constant values for the high-affinity and low-affinity Ca^{2+}-binding sites (K_{d1}) do not change significantly in the presence of saturating amounts of Cu^{2+} (Table 1). These results clearly suggest that both Ca^{2+} and Cu^{2+} can bind simultaneously to S100A13.

It is interesting to explore whether the two metal ions (Ca^{2+} and Cu^{2+}) compete for the same binding sites on the protein. Terbium (Tb^{3+}) is a valuable fluorescent probe that is used to investigate Ca^{2+}-binding properties of proteins (32). Tb^{3+} is known to bind to the Ca^{2+}-binding sites and induce luminescence in the visible region via energy transfer from the aromatic residues in proteins (32). The competition between Ca^{2+} and Cu^{2+} ions to bind to S100A13 was probed by fluorescence energy transfer (FRET) experiments using Tb^{3+}. Fluorescence intensity of Tb^{3+} at 565 nm is observed to progressively increase when S100A13 is titrated with increasing concentrations of $TbCl_3$ (Fig. 6 *A*). The increase in Tb^{3+} fluorescence is compounded by a concomitant decrease in the tryptophan fluorescence intensity at 340 nm (data not shown). The fluorescence energy transfer from the aromatic residues in S100A13 to Tb^{3+} suggests that some of the aromatic residues (Trp and Tyr) are located spatially close to the Ca^{2+} (or Tb^{3+}) binding sites in the protein. The emission intensity at 565 nm is observed to plateau at a S100A13/Tb^{3+} ratio of 1:2, additionally confirming that two Ca^{2+} ions bind per subunit of S100A13 (Fig. 6 *A*, *inset*). The Ca^{2+}-to-S100A13 binding stoichiometry obtained from the Tb^{3+} binding data is consistent with that derived from the ITC experiments. Assuming that the Ca^{2+} and Tb^{3+} binding sites on S100A13 are the same, we measured the binding affinity of Ca^{2+} to S100A13 using the Tb^{3+}-Ca^{2+} competition assay. S100A13, saturated with 2 mM Tb^{3+}, was titrated with increasing concentrations of Ca^{2+} and the binding affinity (K_d) of Ca^{2+} to S100A13 was obtained from the decrease in Tb^{3+} fluorescence at 545 nM. The K_d value estimated for the Ca^{2+}-S100A13 interaction from the Tb^{3+}/Ca^{2+} competition assay ($\sim$25 μM) is in the same range as that obtained from the ITC data ($K_d \sim 8$ μM).

The affinity of S100A13 to Tb^{3+} was examined in the presence of saturating concentrations (2 mM) of Cu^{2+} to assess whether the Ca^{2+} (or Tb^{3+}) competes for the Cu^{2+} sites in the protein. Even at a saturating concentration of Cu^{2+} (2 mM), the fluorescence at 565 nm steadily increases with an increase in the concentration of Tb^{3+}, suggesting that the binding of Ca^{2+} (or Tb^{3+}) and Cu^{2+} to S100A13 are mutually independent (Fig. 6 *B*). The Ca^{2+} (or Tb^{3+})-to-S100A13 binding stoichiometry remains unchanged even in the presence of an excess of Cu^{2+}. On the other hand, S100A13 saturated with Tb^{3+} (2 mM) and titrated with increasing

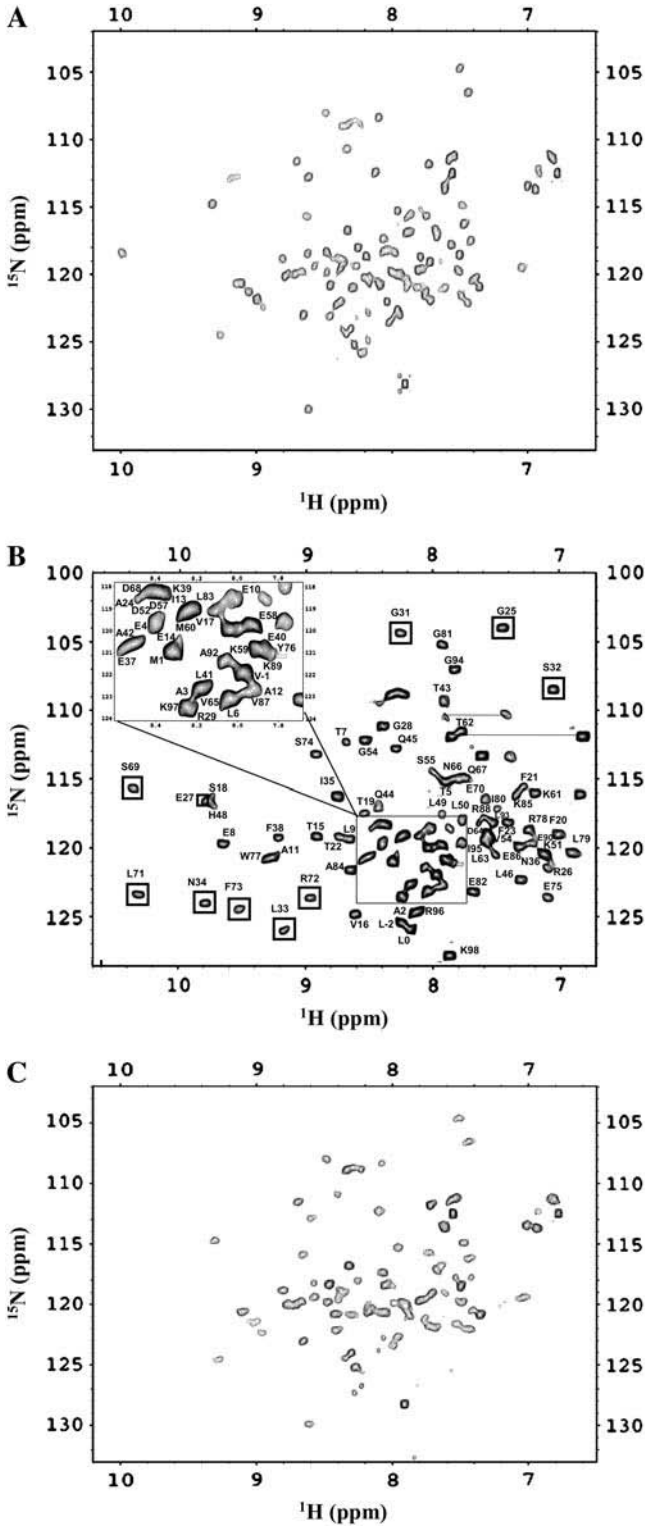

FIGURE 4 ^{1}H-^{15}N HSQC spectra of (*A*) apo-S100A13 and (*B*) S100A13 in the presence of 2 mM $CaCl_2$. (*C*) S100A13 in the presence of 2 mM $CuCl_2$. ^{1}H-^{15}N HSQC spectra were obtained at a protein concentration of 0.1 mM in 25 mM Tris buffer (pH 7.2) containing 25 mM KCl. The buffer solution was prepared in 90% H_2O and 10% D_2O. HSQC spectra were acquired at 25°C. The boxed area represents the crosspeaks of residues that are locating in close proximity to the Ca^{2+}-binding site.

concentrations of Cu^{2+} showed no change in the Tb^{3+} fluorescence intensity at 565 nm (Fig. 6 *C*). These results clearly indicate that Ca^{2+} and Cu^{2+} do not compete with each other for the same binding sites in S100A13. In the event of competition between the metal ions to bind to the same sites on S100A13, the Tb^{3+} fluorescence (at 565 nm) is expected to show a decrease with an increase in concentration of Cu^{2+}.

Interplay between Ca^{2+} and Cu^{2+} binding to S100A13

All the resonances (^{1}H, ^{13}C, and ^{15}N) in the Ca^{2+}-bound state of S100A13 have been assigned (28). The three-dimensional solution structure of S100A13 in the Ca^{2+}-bound state has been reported (15). As for all other S100 proteins, S100A13 also has two distinct Ca^{2+} binding sites. As stated earlier, the Ca^{2+}-binding sites are located in the loops of the two helix-loop-helix motifs. ITC and Tb^{3+}-based fluorescence energy transfer experiments clearly suggest that Cu^{2+} can bind to S100A13 even in the presence of Ca^{2+}. In this context, it would be interesting to identify the Cu^{2+} binding sites on the Ca^{2+}-bound S100A13. Increasing addition of paramagnetic Cu^{2+} results in a progressive decrease in intensity of a few selected crosspeaks in the ^{1}H-^{15}N HSQC spectrum of Ca^{2+}-bound S100A13 (Fig. 7). The residues whose crosspeaks show a significant decrease include Thr-7, Glu-8, Leu-33, Asn-34, His-48, Leu-71, Arg-72, Phe-73, Ser-74, Trp-77, and Arg-78. There is no indication of a major conformational change when Cu^{2+} binds to Ca^{2+}-bound S100A13. The residues that bind to Cu^{2+}, in the Ca^{2+}-bound S100A13 state, appear to be distributed in two locations. One site comprises of Leu-33, Asn-34, Leu-71, and Arg-72, located on the β-sheet between helix-3 and helix-4 (Fig. 8 *A*). The residues in the second Cu^{2+}-binding site include Thr-7, Glu-8, and His-48. These residues are situated in the hinge region between helix-2 and helix-3 and constitute an exclusive Cu^{2+}-binding site (Fig. 8 *B*). Although the first Cu^{2+} binding site partially overlaps with the Ca^{2+} binding site, we believe that the binding of the two kinds of ions to the protein (S100A13) is not mutually exclusive. This notion is supported by the results of the ITC and Tb^{3+} binding experiments, which show that two Cu^{2+} ions bind per monomer of the Ca^{2+}-bound S100A13. In addition, the isocompetition point mass of the Ca^{2+}-bound S100A13 treated with 2 mM Cu^{2+} (after exhaustive dialysis) showed that two Cu^{2+} and two Ca^{2+} ions are simultaneously bound to the protein (data not shown). These results unambiguously demonstrate that S100A13 has distinct Ca^{2+}- and Cu^{2+}-binding sites and, therefore, the binding of one metal ion does not hamper the protein's binding to the other metal ion.

^{1}H-^{15}N HSQC spectra of Cu^{2+}-bound S100A13 at increasing concentrations of Ca^{2+} show a progressive increase in the dispersion of the crosspeaks. The ^{1}H-^{15}N HSQC spectrum of Cu^{2+}-saturated S100A13 in the presence of 2 mM Ca^{2+} mostly resembles the one obtained for the protein

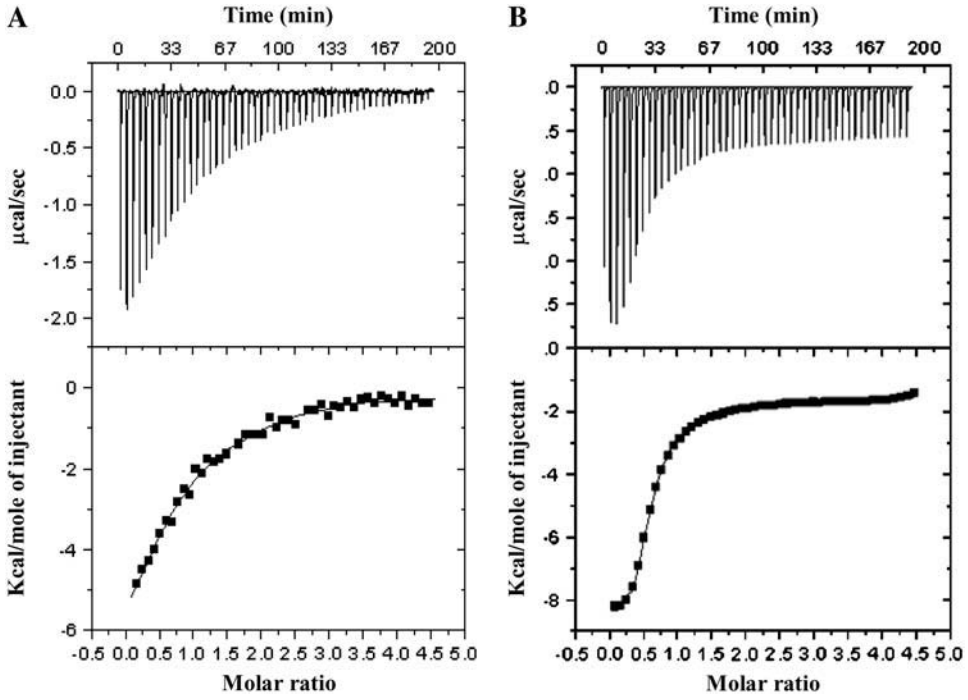

FIGURE 5 Binding curves representing the titration of (*A*) Ca^{2+}-bound S100A13 with Cu^{2+}, (*B*) Cu^{2+}-bound S100A13 with Ca^{2+}. S100A13 was prepared in 25 mM Tris buffer (pH 7.2), containing 25 mM KCl. ITC experiments were performed at 25°C and the data were corrected for heats of dilution and ionization. The upper and lower panels represent the raw data and the best fits of the raw data, respectively. The concentration of S100A13 used was 100 μM.

(S100A13) in the presence of calcium alone. These results suggest that Ca^{2+} not only binds to Cu^{2+}-bound S100A13 but also induces a conformational change that is similar to the one observed when Ca^{2+} binds to the apo-state of the proteins. The effects of Ca^{2+} and Cu^{2+} on the structure of S100A13 appear to be distinctly different. Binding of Cu^{2+} does not result in discernible conformational change(s) in S100A13. On the other hand, Ca^{2+}, upon binding to the apo-S100A13 or the Cu^{2+}-bound S100A13, induces a prominent change(s) in the conformation. Many S100 proteins have been previously shown to bind to transition metals like Zn^{2+} (22). Just as with Ca^{2+}, binding of Zn^{2+} is also known to cause large conformational changes in S100 proteins such as S100B, S100A7, and S100A12 (22). Binding of Zn^{2+} invariably affects Ca^{2+} binding and increases target protein-protein affinities of S100 proteins. In marked contrast, Cu^{2+} appears to play a more docile role as it neither induces a conformational change in S100A13 nor increases the binding affinity of Ca^{2+} to the protein.

Metal binding alters the stability of the protein

Metals not only induce conformational changes but are also known to alter the stability of proteins (33). Investigation of the effect(s) of metal-ion binding may be important to understanding their physiological role(s) in modulating the functional properties of proteins. In this context, we performed thermal denaturation experiments to examine the influence of Ca^{2+} and Cu^{2+} on the thermodynamic stability of apo-S100A13. The far-ultraviolet CD spectrum of S100A13, at 25°C, shows double minima centered at 208 nm and 222 nm (data not shown). These spectral features are consistent with the predominantly helical nature of the protein. Thermal denaturation of apo-S100A13 monitored using ellipticity changes at 222 nm shows that the protein begins to unfold at 68 ± 1°C and complete unfolding occurs beyond 80°C. The apparent T_m (temperature at which 50% of the protein molecules exist in the denatured state(s)) value for the unfolding reaction of apo-S100A13 is estimated to be 76 ± 1°C (Fig. 9 *A*). Interestingly, in the presence of 2 mM Cu^{2+}, the conformational stability of apo-S100A13 is drastically reduced (T_m = 58 ± 1°C). Addition of Ca^{2+} (2 mM) to the apo-S100A13 appears to significantly stabilize the protein (Fig. 9 *A*). The apparent T_m for the unfolding reaction of Ca^{2+}-bound S100A13 is 92 ± 1°C. Treatment of Cu^{2+}-bound S100A13 with 2 mM Ca^{2+} results in an increase in the thermal stability of the protein. The apparent T_m value of the protein is almost similar (T_m = 90 ± 1°C) to the one observed when apo-S100A13 is treated with 2 mM Ca^{2+} alone (Fig. 9 *A*). Surprisingly, the thermodynamic stability of Cu^{2+}-bound S100A13 treated with 2 mM Ca^{2+} is significantly different from that of Ca^{2+}-bound S100A13 treated with 2 mM Cu^{2+}. The T_m of unfolding of the former is ~10°C lower than that of the latter (Fig. 9 *A*). Although two Cu^{2+} ions and two Ca^{2+} ions bind to the protein under both of these conditions, the disparities in stabilities observed could be possibly attributed to the subtle differences in the degree of compactness of the structure of the protein under these two conditions. The structure of the Cu^{2+}-bound S100A13 treated with 2 mM Ca^{2+} appears to be less compact (or less stable) than the structure of the Ca^{2+}-bound S100A13 treated with 2 mM Cu^{2+}. The high conformational flexibility of the Cu^{2+}-bound S100A13 treated with 2 mM Ca^{2+} is supported by results of the amide proton exchange experiments.

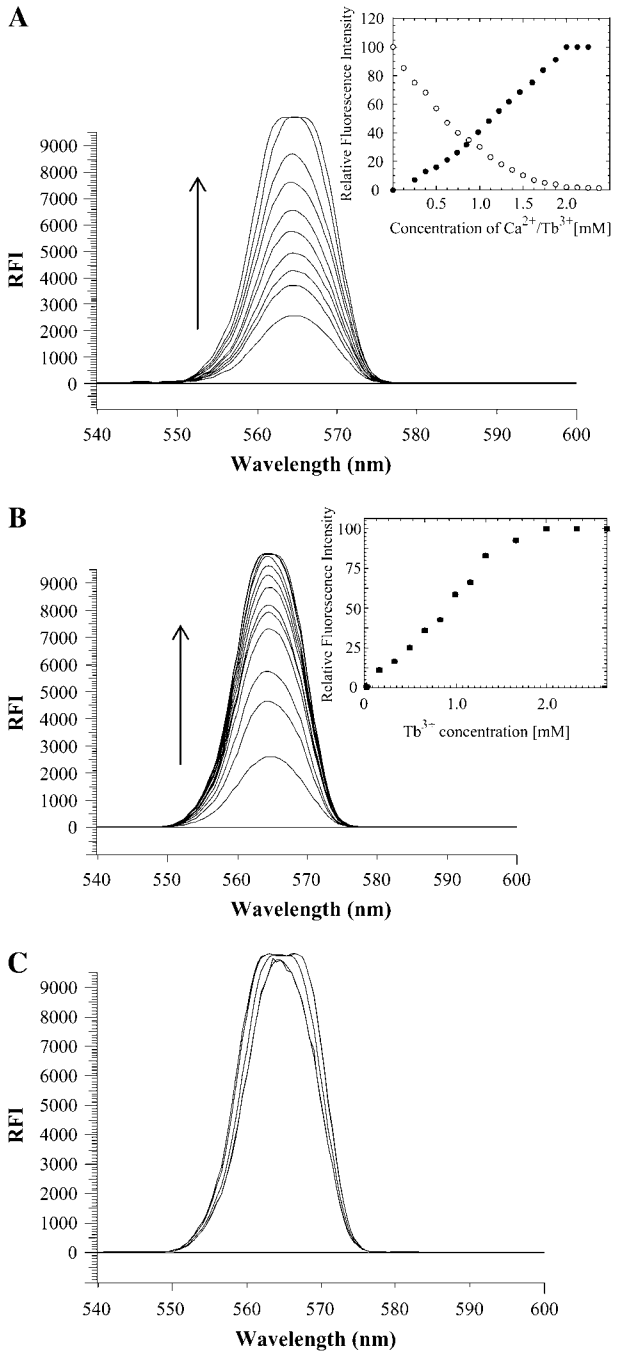

FIGURE 6 Terbium binding to S100A13. (*A*) Titration of apo-S100A13 with increasing concentration of $TbCl_3$. (*Inset*) Titration of apo-S100A13 with increasing concentrations of Tb^{3+} (*solid circle*); S100A13 saturated with Tb^{3+} and titrated with increasing concentrations of $CaCl_2$ (*open circle*) represents change in Tb^{3+} fluorescence (at 545 nm) in the absence (*solid circle*) and presence (*open circle*) of various concentrations of Ca^{2+}. (*B*) Titration of Cu^{2+}-bound S100A13 with increasing concentrations of Tb^{3+}. (*C*) Terbium-bound S100A13 titrated with increasing concentrations of $CuCl_2$. The inset figure in each panel shows the change(s) in the Tb^{3+} emission intensity (at 565 nm) under experimental conditions used in the corresponding panel. The concentration of S100A13 used was 50 μM. All solutions were prepared in 25 mM Tris buffer (pH 7.2, containing 25 mM KCl. The appropriate blank corrections were made in all spectra. The direction of the arrows in *A* and *B* indicate the increase in the Tb^{3+} fluorescence.

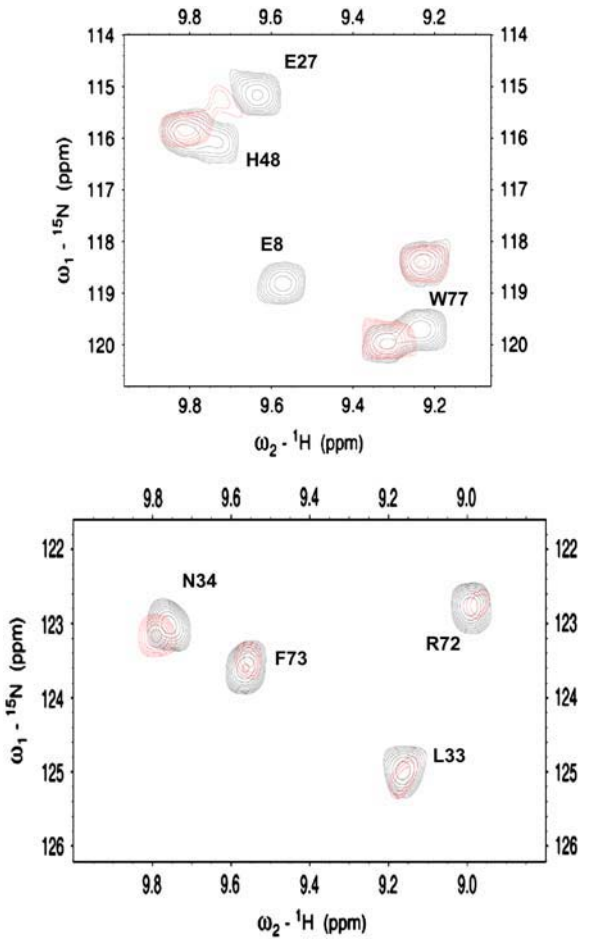

FIGURE 7 Two portions of the overlapped ^1H-^{15}N HSQC spectra of Ca^{2+}-bound S100A13 (*black*) and Ca^{2+}-bound S100A13 in the presence of 2 mM Cu^{2+} (*red*). S100A13 (0.1 mM) was prepared in 25 mM Tris buffer (pH 7.2, dissolved in 90% H_2O + 10% D_2O) containing 25 mM KCl.

Comparison of the ^1H-^{15}N HSQC spectra of S100A13 obtained under these two conditions in D_2O (after incubation of the protein in D_2O for 10 min) clearly shows that most of the residues at the dimer interface and in helix 3 and helix 4 are protected against exchange in S100A13 bound to Ca^{2+} alone (Fig. 9 *B*). Interestingly, in Cu^{2+}-bound S100A13 treated with 2 mM Ca^{2+}, most of the amide protons of residues in these regions are exchanged with D_2O (Fig. 9 *C*). The results of the amide proton exchange are in good agreement with the thermal unfolding experiments and suggest that the final conformational stability of S100A13 is dependent not only on the nature of the metal ions but also on the order in which the metal ions bind to the protein.

S100A13 binds to the C2A domain of synaptotagmin 1 (Syt1)

We had previously demonstrated that the C2A domain synaptotagmin 1 has high binding affinity for Cu^{2+} ($K_{d(app)}$

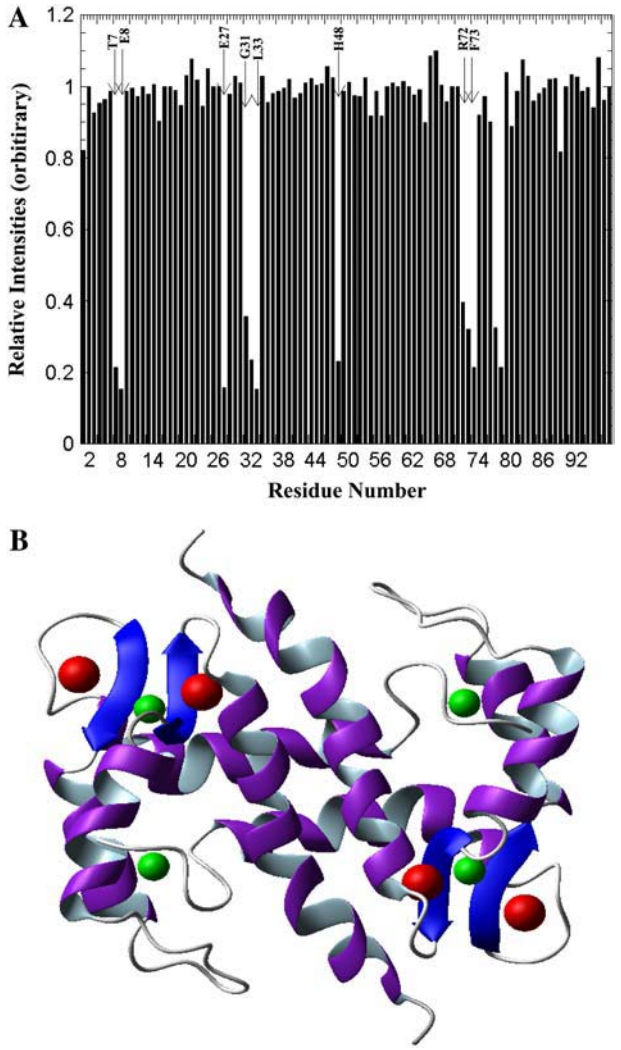

FIGURE 8 (*A*) Chemical shift perturbation plot of Ca^{2+}-bound S100A13 titrated with 2 mM $CuCl_2$. There are two prominent sites (site 1.T7, E8, and H48; site 2.E27, G31, L33, R72, and F73) in the protein at which Cu^{2+} ions appear to bind. The concentration of S100A13 used was 0.1 mM. The protein was prepared in 25 mM Tris buffer (pH 7.2) containing 25 mM KCl and 90% H_2O and 10% D_2O. The experiment was performed at 25°C. (*B*) MOLMOL representation of the backbone fold of S100A13 showing the Cu^{2+} (*green*) and Ca^{2+} (*red*) ions bound to S100A13.

is in the micromolar range (38)). Four Cu^{2+} ions bind per molecule of the C2A domain. No discernible conformational change(s) were observed in the C2A domain upon binding to the metal ion. We performed ITC experiments to examine whether apoS100A13 and the apo-C2A domain interact with each other. The binding isotherm representing the S100A13-C2A titration shows that these proteins interact with each other at a stoichiometric ratio of 1:2 (Fig. 10). Apo-S100A13 binds to the apo-C2A domain with moderate affinity ($K_d \sim 85\ \mu M$) and the binding proceeds with the absorption of heat (Fig. 10). The binding affinity does not change significantly with increase in the NaCl concentration (in the range of 50 to 250 mM, data not shown). In addition, titration

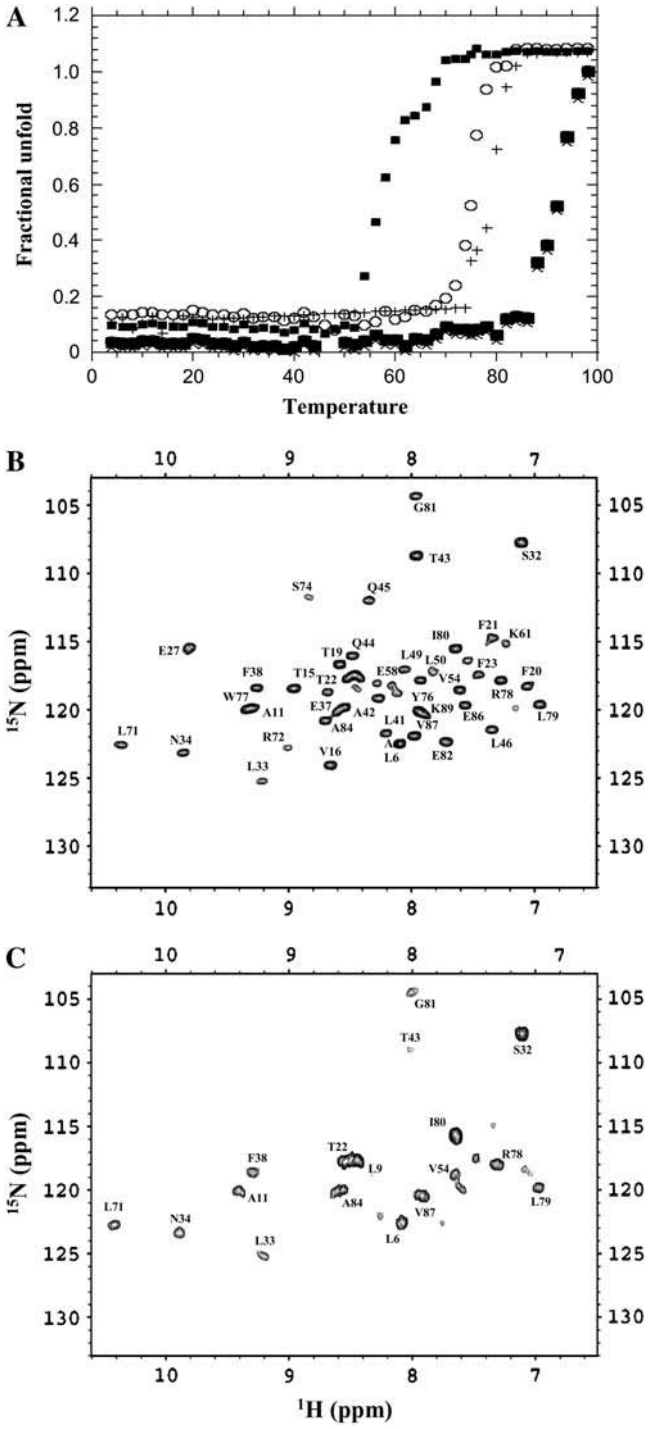

FIGURE 9 (*A*) Thermal unfolding curves of S100A13 monitored by changes in ellipiticity at 222 nm, apo-S100A13 (*open circles*); S100A13 in 2 mM $CaCl_2$ (*solid circles*); S100A13 in 2 mM $CuCl_2$ (*solid triangles*); Cu^{2+}-bound S100A13 treated with 2 mM $CaCl_2$ (*plus symbols*); and Ca^{2+}-bound S100A13 treated with 2 mM $CuCl_2$ (*X*). The concentration of S100A13 used was 0.1 mM. All experiments were performed in 25 mM Tris buffer (pH 7.2) containing 25 mM KCl. Blank corrections were made in all data. (*B* and *C*) ^{1}H-^{15}N HSQC spectra of S100A13 in 2 mM $CaCl_2$ and Cu^{2+}-bound S100A13 treated with 2 mM $CaCl_2$. The ^{1}H-^{15}N HSQC were acquired after 10 min of initiation of deuterium exchange at 25°C. The concentration of the protein used was 0.5 mM.

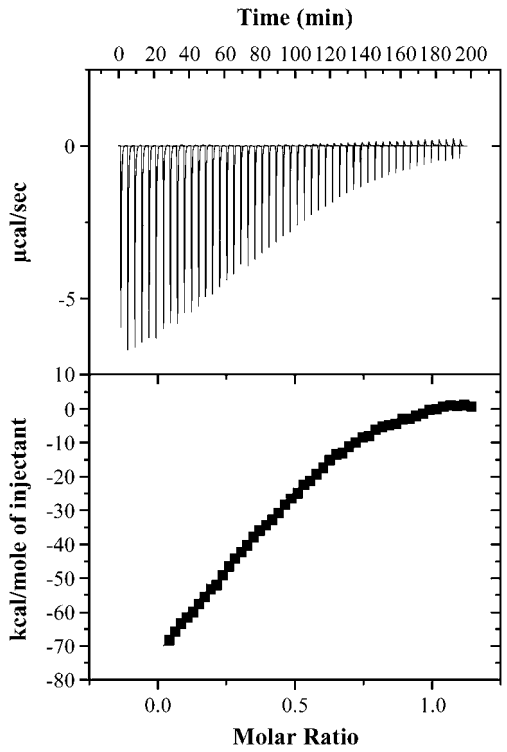

FIGURE 10 Binding isotherm representing the titration of apo-S100A13 with the C2A domain. S100A13 and the C2A domain were prepared in 25 mM Tris buffer (pH 7.2), containing 25 mM KCl. The apparent dissociation constant defining the affinity of the apo-S100A13 to the C2A domain is estimated to be in the micromolar range. ITC experiments were performed at 25°C and the data were corrected for heats of dilution and ionization. The upper and lower panels represent the raw data and the best fits of the raw data, respectively.

of S100A13 and the C2A domain in the presence of excess of Cu^{2+} (2 mM) does appear to affect the binding affinity between these proteins (data not shown). These results suggest that interaction between S100A13 and the C2A domain is not driven by Cu^{2+}.

DISCUSSION

Maciag and coworkers established that Cu^{2+} is mandatory for the secretion of FGF-1 into the extracellular compartment (18). It is believed that the Cu^{2+}-induced oxidation of the thiol group of Cys-30 leading to the formation of the FGF-1 homodimer, is a crucial step in the nonclassical release of FGF-1. However, the source of Cu^{2+} that is required for the oxidation of Cys-30, is still not clear. It is well known that free copper is highly reactive and toxic, and accumulation of the free ionic form of copper is expected to have detrimental effects on the cell (34). To overcome this problem, cells have evolved a mechanism involving small copper-binding proteins called the ''copper chaperones'' (35). These ''copper chaperones'' receive Cu^{2+} from cell-surface copper transporters and distribute them to the destination proteins that require Cu^{2+} for their function(s). Atx1, CCS, and Cox17 are well-studied ''copper chaperones'' found in the cytoplasm of cells (36). Although there is no experimental evidence of any of the ''copper chaperones'' interacting with proteins (such as S100A13 or synaptotagmin) that are involved in the multi-protein FGF release complex, it is reasonable to predict that the Cu^{2+} ions required for the formation of the FGF dimer are transferred from one of the ''copper chaperones'' to proteins involved in the FGF release complex.

Several members of the S100-family have been reported to bind to transition metals like Cu^{2+} and Zn^{2+} (22). Interestingly, S100B and S100A5 play important roles in copper homeostasis as well as in prevention of copper-induced oxidative damage in the brain (3). These S100 proteins, including S100A13, bind to Cu^{2+} with moderate affinity in the micromolar range (22). Interestingly, unlike the Cu^{2+}-binding proteins (like superoxide dismutase, prion proteins, and the ''copper chaperones'' such as Atx1 and CCS), the S100 proteins lack the typical copper-binding motif (37). In this context, it may be worth mentioning that RNase A, which also lacks the typical copper-binding motif, binds to Cu^{2+} (36). Crystal structure of the Cu^{2+}-bound RNaseA revealed that copper binds to the α-amino group of lysine, the carboxyl group of glutamic acid, and the imidazole group of histidine. The Cu^{2+}-binding affinity of S100A13 appears to bear importance in the secretion of FGF-1 through the nonclassical pathway. The Cu^{2+}-binding affinities of the ''copper chaperones'' and S100A13 are similar (in the micromolar range). Therefore, it is possible that S100A13 is the direct recipient of Cu^{2+} from the ''copper chaperones''. The Cu^{2+} bound to S100A13 is possibly then transferred to the C2A domain of synaptotagmin 1 (Syt1). This notion of the transfer of Cu^{2+} from S100A13 to the C2A domain of synaptotagmin is reasonable because 1), ITC experiments show that S100A13 and C2A domain of Syt1 interact with each other with moderate affinity (Fig. 10); 2), the C2A domain binds to Cu^{2+} with very high affinity in the nanomolar range (38); and 3), ITC and ^{1}H-^{15}N HSQC perturbation experiments suggest that the C2A domain binds to FGF-1 (38). As FGF-1 and the C2A domain of Syt1 are involved in direct interaction, the Cu^{2+} bound to the C2A domain is possibly utilized to promote the specific oxidation of Cys-30 in FGF-1 to form the homodimer. At this juncture, the mechanism proposed for the Cu^{2+}-induced FGF homodimer is purely speculative. More detailed structural characterization of the binding interfaces between proteins (S100A13 and FGF-1) involved in the multi-protein FGF release complex is required to validate the proposed mechanism. Also, based on the results of this work, the mutation analysis of Cu^{2+} binding sites of S100A13 will facilitate a better understanding of the role of the metal ion in the nonclassical export of the FGF-1 release complex.

This study was supported by research grants from the National Institutes of Health (NIH NCRR COBRE grant P20RR15569), the Department of Energy (DE-FG02-01ER15161), the Arkansas Biosciences Institute, and the National Science Council, Taiwan (NSC 94-2320-B007-005 and NSC

94-2113-M007-036). I.P. and I.G. were supported by National Institutes of Health grants HL35627, HL32348, and RR1555 (Project 1).

REFERENCES

1. Malmendal, A., C. W. Vander Kooi, N. C. Nielsen, and W. J. Chazin. 2005. Calcium-modulated S100 protein-phospholipid interactions. An NMR study of calbindin D9k and DPC. *Biochemistry.* 44:6502–6512.
2. Bhattacharya, S., C. G. Bunick, and W. J. Chazin. 2004. Target selectivity in EF-hand calcium binding proteins. *Biochim. Biophys. Acta.* 1742:69–79.
3. Wilder, P. T., K. M. Varney, M. B. Weiss, R. K. Gitti, and D. J. Weber. 2005. Solution structure of zinc- and calcium-bound rat S100B as determined by nuclear magnetic resonance spectroscopy. *Biochemistry.* 44:5690–5702.
4. Markowitz, J., R. R. Rustandi, K. M. Varney, P. T. Wilder, R. Udan, S. L. Wu, W. D. Horrocks, and D. J. Weber. 2005. Calcium-binding properties of wild-type and EF-hand mutants of S100B in the presence and absence of a peptide derived from the C-terminal negative regulatory domain of p53. *Biochemistry.* 44:7305–7314.
5. Smith, S. P., and G. S. Shaw. 1998. A change-in-hand mechanism for S100 signalling. *Biochem. Cell Biol.* 76:324–333.
6. Bhattacharya, S., and W. J. Chazin. 2003. Calcium-driven changes in S100A11 structure revealed. *Structure.* 11:738–740.
7. Zimmer, D. B., P. Wright Sadosky, and D. J. Weber. 2003. Molecular mechanisms of S100-target protein interactions. *Microsc. Res. Tech.* 60:552–559.
8. Mueller, A., B. W. Schafer, S. Ferrari, M. Weibel, M. Makek, and C. W. Heizmann. 2005. The calcium-binding protein S100A2 interacts with p53 and modulates its transcriptional activity. *J. Biol. Chem.* 280:29186–29193.
9. Heizmann, C. W., G. Fritz, and B. W. Schafer. 2002. S100 proteins: structure, functions and pathology. *Front. Biosci.* 7:1356–1358.
10. Chan, W. Y., C. L. Xia, D. C. Dong, C. W. Heizmann, and D. T. Yew. 2003. Differential expression of S100 proteins in the developing human hippocampus and temporal cortex. *Microsc. Res. Tech.* 60:600–613.
11. Hsieh, H. L., B. W. Schafer, J. A. Cox, and C. W. Heizmann. 2002. S100A13 and S100A6 exhibit distinct translocation pathways in endothelial cells. *J. Cell Sci.* 115:3149–3158.
12. Marenholz, I., C. W. Heizmann, and G. Fritz. 2004. S100 proteins in mouse and man: from evolution to function and pathology (including an update of the nomenclature). *Biochem. Biophys. Res. Commun.* 322:1111–1112.
13. Nelson, M. R., E. Thulin, P. A. Fagon, S. Forsen, and W. J. Chazin. 2002. The EF-hand domain: a globally cooperative structural unic. *Protein Sci.* 11:198–205.
14. Ridinger, K., B. W. Schafer, I. Durussel, J. A. Cox, and C. W. Heizmann. 2000. S100A13. Biochemical characterization and subcellular localization in different cell lines. *J. Biol. Chem.* 275:8686–8694.
15. Sivaraja, V., T. K. S. Kumar, I. Prudovsky, and C. Yu. 2005. Three-dimensional solution structure of a unique S100 protein. *Biochem. Biophys. Res. Commun.* 335:1140–1148.
16. McClintock, K. A., and G. S. Shaw. 2003. A novel S100 target conformation is revealed by the solution structure of the Ca^{2+}-S100B-TRTK-12 complex. *J. Biol. Chem.* 278:6251–6257.
17. Arnesano, F., L. Banci, I. Bertini, A. Fantoni, L. Tenori, and M. S. Viezzoli. 2005. Structural interplay between calcium(II) and copper(II) binding to S100A13 protein. *Angew. Chem. Int. Ed. Engl.* 39:6341–6344.
18. Prudovsky, I., A. Mandinova, R. Soldi, C. Bagala, I. Graziani, M. Landriscina, F. Tarantini, M. Duarte, S. Bellum, H. Doherty, and T. Maciag. 2003. The non-classical export routes: FGF1 and IL-1alpha point the way. *J. Cell Sci.* 116:4871–4881.
19. Arunkumar, A. I., S. Srisailam, T. K. S. Kumar, K. M. Kathir, Y. H. Chi, H. M. Wang, G. G. Chang, I. Chiu, and C. Yu. 2002. Structure and stability of an acidic fibroblast growth factor from *Notophthalmus viridescens*. *J. Biol. Chem.* 277:46424–46432.
20. Landriscina, M., C. Bagala, A. Mandinova, R. Soldi, I. Micucci, S. Bellum, I. Prudovsky, and T. Maciag. 2001. Copper induces the assembly of a multiprotein aggregate implicated in the release of fibroblast growth factor 1 in response to stress. *J. Biol. Chem.* 276:25549–25557.
21. Landricina, M., R. Soldi, C. Bagala, I. Miccuci, S. Bellum, F. Tarantini, I. Prudovsky, and T. Maciag. 2001. S100A13 participates in the release of fibroblast growth factor 1 in response to heat shock in vitro. *J. Biol. Chem.* 276:22544–22552.
22. Heizmann, C. W., and J. A. Cox. 1998. New perspectives on S100 proteins: a multi-functional Ca(II)-, Zn(II)- and Cu(II)-binding protein family. *Biometals.* 11:383–397.
23. Pierce, M. M., C. S. Raman, and B. T. Nall. 1999. Isothermal titration calorimetry of protein-protein interactions. *Methods.* 2:213–221.
24. Jackson, M., S. Chopra, R. D. Smiley, P. O. A. Maynord, A. Rosowsky, R. E. London, L. Levy, T. I. Kalman, and E. E. Howell. 2005. Calorimetric studies of ligand binding in R67 dihydrofolate reductase. *Biochemistry.* 37:12420–12433.
25. Gao, X., K. Bain, J. B. Bonanno, M. Buchanan, D. Henderson, D. Lorimer, C. Marsh, J. A. Reynes, J. M. Sauder, K. Schwinn, C. Thai, and S. K. Burley. 2005. High-throughput limited proteolysis/mass spectrometry for protein domain elucidation. *J. Struct. Funct. Genomics.* 2–3:129–134.
26. Kathir, K. M., T. K. S. Kumar, D. Rajalingam, and C. Yu. 2005. Time-dependent changes in the denatured state(s) influence the folding mechanism of an all β-sheet protein. *J. Biol. Chem.* 280:29682–29688.
27. Hajuduk, P. J., R. P. Meadows, and S. W. Fesik. 1999. NMR-based screening in drug discovery. *Q. Rev. Biophys.* 32:211–240.
28. Sivaraja, V., T. K. S. Kumar, and C. Yu. 2005. Resonance assignments for mouse S100A13. *J. Biomol. NMR.* 3:257.
29. Bertini, I., C. Luchinat, G. Parigi, and R. Pierattelli. 2005. NMR spectroscopy of Paramagnetic metlloproteins. *ChemBioChem.* 6:1536–1549.
30. Pintacuda, G., and G. Otting. 2002. Identification of protein surfaces by NMR measurements with a paramagnetic Gd(III) chelate. *J. Am. Chem. Soc.* 3:372–373.
31. Ye, Y., H. W. Lee, W. Yang, S. Shealy, and J. J. Yang. 2005. Probing site-specific calmodulin calcium and lanthanide affinity by grafting. *J. Am. Chem. Soc.* 11:3743–3750.
32. Jobby, M. K., and Y. Sharma. 2005. Calcium-binding crystallins from Yersinia pestis. Characterization of two single betagamma-crystallin domains of a putative exported protein. *J. Biol. Chem.* 280:1209–1216.
33. Spinozzi, F., S. Gatto, V. DeFilippis, F. Carsughi, P. DiMuro, and F. Beltramini. 2005. Contribution of the copper ions in the dinuclear active site to the stability of *Carcinus aestuarii* hemocyanin. *Arch. Biochem. Biophys.* 439:42–52.
34. Luk, E., L. T. Jensen, and V. C. Culotta. 2003. The many highways for intracellular trafficking of metals. *J. Biol. Inorg. Chem.* 8:803–809.
35. Pufahl, R. A., C. Singer, K. L. Peariso, S. J. Lin, P. Schimdt, C. Fahrni, V. C. Cullotta, J. E. Penner-Hahn, and T. V. O'Halloran. 1997. Metal ion chaperone function of the soluble Cu(I) receptor Atx1. *Science.* 278:853–856.
36. Finney, L. A., and T. V. O'Halloran. 2003. Transition metal speciation in the cell: insights from the chemistry of metal ion receptors. *Science.* 300:931–936.
37. Gaggelli, E., F. Bernardi, E. Molteni, R. Pogni, D. Valensin, G. Valensin, M. Remelli, M. Luczkowski, and H. Kozlowski. 2005. Interaction of the human prion PrP(106–126) sequence with copper(II), manganese(II), and zinc(II): NMR and EPR studies. *J. Am. Chem. Soc.* 3:996–1006.
38. Rajalingam, D., T. K. S. Kumar, and C. Yu. 2005. C2A domain of synaptotagmin exhibits high binding affinity for copper. Implications in the formation of the multiprotein FGF release complex. *Biochemistry.* 44:14431–14442.